# AN ADAPTIVE $P_1$ FINITE ELEMENT METHOD FOR TWO-DIMENSIONAL MAXWELL'S EQUATIONS*

S.C. BRENNER, J. GEDICKE, AND L.-Y. SUNG

Abstract. Recently a new numerical approach for two-dimensional Maxwell's equations based on the Hodge decomposition for divergence-free vector fields was introduced by Brenner et al. In this paper we present an adaptive $P_1$ finite element method for two-dimensional Maxwell's equations that is based on this new approach. The reliability and efficiency of *a posteriori* error estimators based on the residual and the dual weighted-residual are verified numerically. The performance of the new approach is shown to be competitive with the lowest order edge element of Nédélec's first family.

## 1. Introduction

Recently Brenner et al. [8] introduced a new approach for solving two-dimensional Maxwell's equations that is based on the Hodge (Helmholtz) decomposition for divergence-free vector fields. It reduces the boundary value problem for Maxwell's equations to several scalar second order elliptic boundary value problems, which can be discretized by standard $P_1$ finite element methods. In this paper we develop *a posteriori* error estimators for the new approach. The $L_2$ error for the approximation of the solution $\mathbf{u}$ of the Maxwell equations is shown to be bounded by a residual type error estimator [1, 6, 13, 27], and we consider two types of error estimators for the $L_2$ error of the approximation of $\nabla \times \mathbf{u}$. For convex domains we have an $L_2$-type residual error estimator. For general domains we propose an error estimator based on the dual weighted-residual (DWR) approach of Becker and Rannacher [2, 4]. We present numerical results that verify the reliability of the *a posteriori* error estimators and demonstrate their efficiency. The convergence of adaptive methods based on these error estimators is of optimal order.

*Key words and phrases.* Adaptivity, Error estimates, Finite element method, Hodge decomposition, Maxwell's equations,

* This work was supported in part by the National Science Foundation under Grant No. DMS-07-13835 and Grand No. DMS-10-16332. The second author was additionally supported by the DFG Research Center MATHEON "Mathematics for Key Technologies" and the DFG graduate school BMS "Berlin Mathematical School".

Published in Journal of Scientific Computing, 55:738–754, 2013. The final publication is available at Springer via http://dx.doi.org/10.1007/s10915-012-9658-8.

Compared with the discretization of Maxwell's equations by the lowest order edge element of Nédélec's first family [23] which has one degree of freedom per edge, this new discretization leads to smaller but multiple discrete systems. However, most of these systems can be solved in parallel and the new approach leads to comparable or better results as shown empirically by our numerical experiments. We note that the adaptive finite element method (AFEM) for the lowest order edge element has been studied in [3, 5, 14, 15, 21, 25].

We now introduce the model problem and briefly recall the Hodge decomposition approach in [8]. The model problem seeks a solution $\mathbf{u} \in H_0(\mathrm{curl};\Omega) \cap H(\mathrm{div}^0;\Omega)$ such that

$$(\nabla \times \mathbf{u}, \nabla \times \mathbf{v}) + \alpha(\mathbf{u},\mathbf{v}) = (\mathbf{f},\mathbf{v}) \ \forall \mathbf{v} \in H_0(\mathrm{curl};\Omega) \cap H(\mathrm{div}^0;\Omega) \tag{1}$$

for a bounded polygonal domain $\Omega \subset \mathbb{R}^2$ and $\mathbf{f} \in [L_2(\Omega)]^2$. Here $(\cdot,\cdot)$ denotes the $L_2$ inner product over $\Omega$ and the space $H_0(\mathrm{curl};\Omega)$ is defined by

$$H_0(\mathrm{curl};\Omega) := \left\{\mathbf{v} \in [L_2(\Omega)]^2 : \nabla \times \mathbf{v} \in L_2(\Omega) \text{ and } \mathbf{n} \times \mathbf{v} = 0 \text{ on } \partial\Omega\right\},$$

where $\nabla \times \mathbf{v} = \mathrm{curl}\,\mathbf{v} = (\partial v_2/\partial x_1) - (\partial v_1/\partial x_2)$ and $\mathbf{n}$ denotes the outer unit normal along $\partial\Omega$. The space $H(\mathrm{div}^0;\Omega)$ is defined by

$$H(\mathrm{div}^0;\Omega) := \left\{\mathbf{v} \in [L_2(\Omega)]^2 : \nabla \cdot \mathbf{v} = 0\right\},$$

where $\nabla \cdot \mathbf{v} = \mathrm{div}\,\mathbf{v} = (\partial v_1/\partial x_1) + (\partial v_2/\partial x_2)$.

The problem (1) is related to the time-harmonic Maxwell equations for $\alpha \le 0$ and the time-domain Maxwell equations for $\alpha > 0$ [7, 9, 10, 16, 20, 22]. In the following it is assumed that problem (1) admits a unique solution. Thus $-\alpha$ is not a Maxwell eigenvalue and in particular $\alpha \neq 0$ if $\Omega$ is not simply connected.

Using the Hodge (Helmholtz) decomposition for $H(\mathrm{div}^0;\Omega)$, we can write

$$\mathbf{u} = \nabla \times \phi + \sum_{j=1}^{m} c_j \nabla \varphi_j, \tag{2}$$

where $\phi \in H^1(\Omega)$ satisfies $(\phi, 1) = 0$, $\nabla \times \phi = [\partial\phi/\partial x_2, -\partial\phi/\partial x_1]^t$, $m \ge 0$ is the Betti number for $\Omega$ ($m = 0$ if $\Omega$ is simply connected), and the functions $\varphi_1, \ldots, \varphi_m$ are defined as follows.

Let the outer boundary of $\Omega$ be denoted by $\Gamma_0$ and the $m$ components of the inner boundary be denoted by $\Gamma_1, \ldots, \Gamma_m$. Then the functions $\varphi_j \in H^1(\Omega)$ are determined by the scalar problems

$$(\nabla\varphi_j, \nabla v) = 0 \quad \forall v \in H_0^1(\Omega), \quad \varphi_j|_{\Gamma_0} = 0 \text{ and } \varphi_j|_{\Gamma_k} = \delta_{jk}, \tag{3}$$

where $\delta_{jk} = 1$ if $j = k$ and $\delta_{jk} = 0$ if $j \neq k$ for $1 \le j, k \le m$.

The function $\phi$ in (2) is determined by

$$(\nabla \times \phi, \nabla \times \psi) = (\xi, \psi) \quad \forall \psi \in H^1(\Omega) \tag{4}$$

with the constraint $(\phi, 1) = 0$, where the function $\xi = \nabla \times \mathbf{u} \in H^1(\Omega)$ is determined by

$$(\nabla \times \xi, \nabla \times \psi) + \alpha(\xi, \psi) = (\mathbf{f}, \nabla \times \psi) \quad \forall \psi \in H^1(\Omega) \tag{5}$$

when $\alpha \neq 0$, and by (5) together with the constraint $(\xi, 1) = 0$ when $\Omega$ is simply connected and $\alpha = 0$.

*Remark* 1. Note that

$$(\nabla \times v, \nabla \times w) = (\nabla v, \nabla w) \quad \forall v, w \in H^1(\Omega)$$

and the problems (4) and (5) are standard Neumann boundary value problems for the Laplace operator.

In the case $m \geq 1$ the coefficients $c_j$ in (2) are determined by the symmetric positive-definite system

$$\sum_{j=1}^{m} (\nabla \varphi_j, \nabla \varphi_k) c_j = \frac{1}{\alpha} (\mathbf{f}, \nabla \varphi_k) \quad \text{for } 1 \leq k \leq m.$$

Let $V_h \subset H^1(\Omega)$ be a finite element space and $\mathring{V}_h = V_h \cap H_0^1(\Omega)$. It is shown in [8] that (1) can be solved by the following procedure.

- First we compute $\xi_h \in V_h$, which provides an approximation of $\nabla \times \mathbf{u}$, by solving the discrete problem

$$(\nabla \times \xi_h, \nabla \times \psi_h) + \alpha(\xi_h, \psi_h) = (\mathbf{f}, \nabla \times \psi_h) \quad \forall \psi_h \in V_h \tag{6}$$

  when $\alpha \neq 0$, and by solving (6) together with the constraint $(\xi_h, 1) = 0$ when $\Omega$ is simply connected and $\alpha = 0$.
- Then we compute $\phi_h \in V_h$ by solving the discrete problem

$$(\nabla \times \phi_h, \nabla \times \psi_h) = (\xi_h, \psi_h) \quad \forall \psi_h \in V_h \tag{7}$$

  with the constraint $(\phi_h, 1) = 0$.
- If $\Omega$ is not simply connected ($m \geq 1$), we compute the functions $\varphi_{1,h}, \ldots, \varphi_{m,h} \in V_h$ by solving the discrete problems

$$(\nabla \varphi_{j,h}, \nabla v_h) = 0 \quad \forall v_h \in \mathring{V}_h, \quad \varphi_{j,h}|_{\Gamma_0} = 0 \text{ and } \varphi_{j,h}|_{\Gamma_k} = \delta_{jk}, \tag{8}$$

  and we compute the coefficients $c_{j,h}$ for $1 \leq j \leq m$ by

$$\sum_{j=1}^{m} (\nabla \varphi_{j,h}, \nabla \varphi_{k,h}) c_{j,h} = \frac{1}{\alpha} (\mathbf{f}, \nabla \varphi_{k,h}) \quad \text{for } 1 \leq k \leq m. \tag{9}$$

- The approximation of $\mathbf{u}$ is given by

$$\mathbf{u}_h = \nabla \times \phi_h + \sum_{j=1}^{m} c_{j,h} \nabla \varphi_{j,h}. \tag{10}$$

The rest of the paper is organized as follows. We construct the error estimators in Section 2 where we also provide some analysis. The adaptive finite element method is described in Section 3. In Section 4

we present numerical results that demonstrate the reliability and efficiency of the proposed error estimators, and we also compare the new approach with the discretization by the lowest order edge element in Nédélec's first family. We end with some concluding remarks in Section 5.

## 2. A posteriori error estimators

In this section we construct an *a posteriori* error estimator for the error $\|\mathbf{u}-\mathbf{u}_h\|_{L_2(\Omega)}$ and two *a posteriori* error estimators for the error $\|\xi-\xi_h\|_{L_2(\Omega)}$.

Let $\mathcal{T}_h$ be a triangulation of $\Omega$ and

$$V_h=\left\{v\in H^1(\Omega): v|_T\in P_1(T)\ \forall T\in\mathcal{T}_h\right\},$$

where $P_1(T)$ denotes the space of affine functions on a triangle $T$. We will denote the set of the edges of the triangles in $\mathcal{T}_h$ by $\mathcal{E}_h$ and the set of the edges interior to $\Omega$ by $\mathcal{E}_h^i$.

Let $[\![v]\!]:=v|_{T_+}-v|_{T_-}$ denote the jump over the edge $E=T_+\cap T_-$ for $T_\pm\in\mathcal{T}_h$ and $[\![v]\!]:=v|_{T_+}$ on boundary edges. Let $n_E=[n_1,n_2]^t$ denote the unit normal vector pointing from $T_+$ to $T_-$ and $t_E=[-n_2,n_1]^t$ denote the unit tangent vector to $E$. The length of an edge is denoted by $h_E$ and $h_T:=\operatorname{diam} T$. In the following, the notation $x\lesssim y$ abbreviates the inequality $x\le Cy$ with a constant $C>0$ that does not depend on the mesh size.

Our first observation is that the $L_2$ error of $\mathbf{u}_h$ is controlled by the $H^1$ error of $\phi_h$ and the $H^1$ errors of $\varphi_{j,h}$ for $1\le j\le m$.

**Lemma 1.** *Let $\boldsymbol{u}_h$ be the approximation of $\boldsymbol{u}$ given by* (10)*. We have*

$$\|\boldsymbol{u}-\boldsymbol{u}_h\|_{L_2(\Omega)}\lesssim\|\nabla\times(\phi-\phi_h)\|_{L_2(\Omega)}+\sum_{j=1}^m\|\nabla(\varphi_j-\varphi_{j,h})\|_{L_2(\Omega)}.$$

*Proof.* It follows from (10) and the triangle inequality that

$$\begin{aligned}\|\mathbf{u}-\mathbf{u}_h\|_{L_2(\Omega)}&\le\|\nabla\times(\phi-\phi_h)\|_{L_2(\Omega)}+\sum_{j=1}^m\|c_j\nabla\varphi_j-c_{j,h}\nabla\varphi_{j,h}\|_{L_2(\Omega)}\\&\le\|\nabla\times(\phi-\phi_h)\|_{L_2(\Omega)}+\sum_{j=1}^m\big(|c_j|\|\nabla(\varphi_j-\varphi_{j,h})\|_{L_2(\Omega)}\\&\quad+|c_j-c_{j,h}|\|\nabla\varphi_j\|_{L_2(\Omega)}+|c_j-c_{j,h}|\|\nabla(\varphi_j-\varphi_{j,h})\|_{L_2(\Omega)}\big),\end{aligned}$$

and the arguments in the proofs of [8, Lemmas 4.6 and 4.7] lead to the estimates

$$|c_j|\lesssim\|f\|_{L_2(\Omega)}$$

and

$$|c_j-c_{j,h}|\lesssim\max_{1\le j\le m}\|\nabla(\varphi_j-\varphi_{j,h})\|_{L_2(\Omega)}\le\sum_{j=1}^m\|\nabla(\varphi_j-\varphi_{j,h})\|_{L_2(\Omega)}.\ \square$$

Next we construct error estimators for $\|\nabla\times(\phi-\phi_h)\|_{L_2(\Omega)}$ and $\|\nabla(\varphi_j-\varphi_{j,h})\|_{L_2(\Omega)}$.

**Lemma 2.** *Let $\varphi_{j,h}\in V_h$, $j=1,\ldots,m$, be the solutions of* (8). *We have*

$$\|\nabla(\varphi_j-\varphi_{j,h})\|^2_{L_2(\Omega)}\lesssim\sum_{E\in\mathcal{E}_h^i}h_E\|[\![\nabla\varphi_{j,h}]\!]\cdot n_E\|^2_{L_2(E)}.$$

*Proof.* Define the residual $\mathrm{Res}_h(v):=-(\nabla\varphi_{j,h},\nabla v)$ for all $v\in H_0^1(\Omega)$ and let $\|\mathrm{Res}_h\|_*$ denote the dual norm of the residual with respect to $H_0^1(\Omega)$. Since $\varphi_j-\varphi_{j,h}\in H_0^1(\Omega)$, it follows from (3) that

$$\begin{aligned}\|\nabla(\varphi_j-\varphi_{j,h})\|^2_{L_2(\Omega)}&=(\nabla\varphi_j-\nabla\varphi_{j,h},\nabla(\varphi_j-\varphi_{j,h}))\\&=-(\nabla\varphi_{j,h},\nabla(\varphi_j-\varphi_{j,h}))\\&=\mathrm{Res}_h(\varphi_j-\varphi_{j,h})\lesssim\|\mathrm{Res}_h\|_*\|\nabla(\varphi_j-\varphi_{j,h})\|_{L_2(\Omega)}.\end{aligned}$$

Let $v\in H_0^1(\Omega)$ be arbitrary and $v_h\in\mathring{V}_h$ be its Scott-Zhang interpolant [11, 26] so that

$$\sum_{E\in\mathcal{E}_h}\|h_E^{-1/2}(v-v_h)\|^2_{L_2(E)}\lesssim\|\nabla v\|^2_{L_2(\Omega)}. \tag{11}$$

Since $\mathrm{Res}_h|_{\mathring{V}_h}=0$ by (8), we have

$$\begin{aligned}\mathrm{Res}_h(v)&=\mathrm{Res}_h(v-v_h)=-(\nabla\varphi_{j,h},\nabla(v-v_h))\\&=-\sum_{E\in\mathcal{E}_h^i}\int_E h_E^{1/2}([\![\nabla\varphi_{j,h}]\!]\cdot n_E)h_E^{-1/2}(v-v_h)ds,\end{aligned}$$

which together with the interpolation estimate (11) and the Cauchy-Schwarz inequality yields

$$\|\mathrm{Res}_h\|_*\lesssim\left(\sum_{E\in\mathcal{E}_h^i}h_E\|[\![\nabla\varphi_{j,h}]\!]\cdot n_E\|^2_{L_2(E)}\right)^{1/2}.$$ □

**Lemma 3.** *Let $\phi_h$ be the solution of* (7). *We have*

$$\begin{aligned}&\|\nabla\times(\phi-\phi_h)\|^2_{L_2(\Omega)}\\&\quad\lesssim\sum_{T\in\mathcal{T}_h}h_T^2\|\xi_h\|^2_{L_2(T)}+\sum_{E\in\mathcal{E}_h}h_E\|[\![\nabla\times\phi_h]\!]\cdot t_E\|^2_{L_2(E)}+\|\xi-\xi_h\|^2_{L_2(\Omega)},\end{aligned}$$

*where $\xi_h$ is the solution of* (6).

*Proof.* It follows from (4) that

$$\begin{aligned}\|\nabla\times(\phi-\phi_h)\|^2_{L_2(\Omega)}&=-(\nabla\times\phi_h,\nabla\times(\phi-\phi_h))+(\xi,\phi-\phi_h)\\&=\mathrm{Res}_h(\phi-\phi_h)+(\xi-\xi_h,\phi-\phi_h),\end{aligned}$$

where the residual is defined by

$$\mathrm{Res}_h(v):=(\xi_h,v)-(\nabla\times\phi_h,\nabla\times v)\quad\forall v\in H^1(\Omega).$$

Therefore we have

$$\|\nabla\times(\phi-\phi_h)\|^2_{L_2(\Omega)} \lesssim \|\mathrm{Res}_h\|_*\|\nabla\times(\phi-\phi_h)\|_{L_2(\Omega)} + \|\xi-\xi_h\|_{L_2(\Omega)}\|\phi-\phi_h\|_{L_2(\Omega)},$$

where $\|\mathrm{Res}_h\|_*$ is the dual norm of the residual with respect to $H^1(\Omega)$. Note that $(\phi-\phi_h,1)=0$ and hence we can apply Friedrichs' inequality to obtain

$$\|\nabla\times(\phi-\phi_h)\|_{L_2(\Omega)} \lesssim \|\mathrm{Res}_h\|_* + \|\xi-\xi_h\|_{L_2(\Omega)}.$$

Let $v\in H^1(\Omega)$ be arbitrary and $v_h\in V_h$ be its Scott-Zhang interpolant [11, 26] so that

$$\sum_{T\in\mathcal{T}_h}\|h_T^{-1}(v-v_h)\|^2_{L_2(T)} + \sum_{E\in\mathcal{E}_h}\|h_E^{-1/2}(v-v_h)\|^2_{L_2(E)} \lesssim \|\nabla v\|^2_{L_2(\Omega)}. \tag{12}$$

It follows from (7) and integration by parts that

$$\begin{aligned}\mathrm{Res}_h(v) &= (\xi_h, v-v_h) - (\nabla\times\phi_h, \nabla\times(v-v_h))\\ &= \sum_{T\in\mathcal{T}_h}\int_T h_T\xi_h h_T^{-1}(v-v_h)dx\\ &\quad + \sum_{E\in\mathcal{E}_h}\int_E h_E^{1/2}([\![\nabla\times\phi_h]\!]\cdot t_E)h_E^{-1/2}(v-v_h)ds,\end{aligned}$$

which together with the Cauchy-Schwarz inequality and the interpolation estimates (12) yields

$$\|\mathrm{Res}_h\|_* \lesssim \left(\sum_{T\in\mathcal{T}_h} h_T^2\|\xi_h\|^2_{L_2(T)}\right)^{1/2} + \left(\sum_{E\in\mathcal{E}_h} h_E\|[\![\nabla\times\phi_h]\!]\cdot t_E\|^2_{L_2(E)}\right)^{1/2}.\square$$

Combining Lemmas 1, 2 and 3, we obtain the following result.

**Theorem 1.** *Let $\boldsymbol{u}_h$ be the approximation of $\boldsymbol{u}$ given by* (10)*. We have*

$$\|\boldsymbol{u}-\boldsymbol{u}_h\|_{L_2(\Omega)} \lesssim \eta_R + \|\xi-\xi_h\|_{L_2(\Omega)},$$

*where*

$$\begin{aligned}\eta_R^2 &:= \sum_{T\in\mathcal{T}_h} h_T^2\|\xi_h\|^2_{L_2(T)} + \sum_{E\in\mathcal{E}_h} h_E\|[\![\nabla\times\phi_h]\!]\cdot t_E\|^2_{L_2(E)}\\ &\quad + \sum_{j=1}^m\sum_{E\in\mathcal{E}_h^i} h_E\|[\![\nabla\varphi_{j,h}]\!]\cdot n_E\|^2_{L_2(E)}.\end{aligned} \tag{13}$$

*Remark* 2. If $\mathbf{f}$ is a piecewise smooth vector field, then $\|\xi-\xi_h\|_{L_2(\Omega)}$ is of higher order compared with $\|\mathbf{u}-\mathbf{u}_h\|_{L_2(\Omega)}$ (cf. [8, Remark 4.4]). This is the case for the numerical examples in Section 4, where $\|\xi-\xi_h\|_{L_2(\Omega)}$ can be safely ignored in the evaluation of $\eta_R$.

*Remark* 3. The efficiency of individual terms of the error estimator $\eta_R$ can be established by the bubble function techniques of Verfürth (cf. [1, 27]). However it is not clear whether the efficiency of $\eta_R$ as a whole can also be established by such techniques.

Finally we consider error estimators for $\|\xi - \xi_h\|_{L_2(\Omega)}$, where we assume that $\mathbf{f}|_T \in [H^\beta(T)]^2 \cap H(\mathrm{curl}; T)$ for all $T \in \mathcal{T}_h$ and for some $\beta \in (1/2, 1]$. Since $(\xi - \xi_h, 1) = 0$, there exists a solution $\zeta$ of the dual problem

$$(\nabla \times \zeta, \nabla \times v) + \alpha(\zeta, v) = (\xi - \xi_h, v) \quad \forall v \in H^1(\Omega) \tag{14}$$

that satisfies the constraint $(\zeta, 1) = 0$. Therefore we can write

$$\begin{aligned}\|\xi - \xi_h\|^2_{L_2(\Omega)} &= (\nabla \times \zeta, \nabla \times (\xi - \xi_h)) + \alpha(\zeta, \xi - \xi_h) \\ &= (\nabla \times (\zeta - \zeta_h), \nabla \times (\xi - \xi_h)) + \alpha(\zeta - \zeta_h, \xi - \xi_h),\end{aligned}$$

for all $\zeta_h \in V_h$, where we have also used the Galerkin orthogonality (cf. (5) and (6))

$$(\nabla \times (\xi - \xi_h), \nabla \times v_h) + \alpha(\xi - \xi_h, v_h) = 0 \quad \forall v_h \in V_h.$$

It then follows from (5) and integration by parts that

$$\begin{aligned}\|\xi - \xi_h\|^2_{L_2(\Omega)} &= (\nabla \times (\zeta - \zeta_h), \mathbf{f} - \nabla \times \xi_h) - \alpha(\zeta - \zeta_h, \xi_h) \\ &= \sum_{T \in \mathcal{T}_h} \int_T [\nabla \times (\zeta - \zeta_h) \cdot (\mathbf{f} - \nabla \times \xi_h) - \alpha(\zeta - \zeta_h)\xi_h]\, dx \\ &= \sum_{T \in \mathcal{T}_h} \int_T (\nabla \times \mathbf{f} - \alpha\xi_h)(\zeta - \zeta_h) dx \\ &\quad - \sum_{E \in \mathcal{E}_h} \int_E (\llbracket \mathbf{f} - \nabla \times \xi_h \rrbracket \cdot t_E)(\zeta - \zeta_h) ds,\end{aligned} \tag{15}$$

which is valid for any $\zeta_h \in V_h$.

If $\Omega$ is convex, then the solution $\zeta$ of the dual problem (14) belongs to $H^2(\Omega)$ [19] and

$$\|\zeta\|_{H^2(\Omega)} \lesssim \|\xi - \xi_h\|_{L_2(\Omega)}.$$

In this case we can take $\zeta_h \in V_h$ to be the nodal interpolant of $\zeta$ and we have [11, 17]

$$\sum_{T \in \mathcal{T}_h} \|h_T^{-2}(\zeta - \zeta_h)\|^2_{L_2(T)} + \sum_{E \in \mathcal{E}_h} \|h_E^{-3/2}(\zeta - \zeta_h)\|^2_{L_2(E)} \lesssim \|\xi - \xi_h\|_{L_2(\Omega)}. \tag{16}$$

Combining (15) and (16) with the Cauchy-Schwarz inequality, we find

$$\|\xi - \xi_h\|_{L_2(\Omega)} \lesssim \eta_{reg}, \tag{17}$$

where

$$\eta^2_{reg} := \sum_{T \in \mathcal{T}_h} h_T^4 \|\nabla \times \mathbf{f} - \alpha\xi_h\|^2_{L_2(T)} + \sum_{E \in \mathcal{E}_h} h_E^3 \|\llbracket \mathbf{f} - \nabla \times \xi_h \rrbracket \cdot t_E\|^2_{L_2(E)}. \tag{18}$$

For a nonconvex domain $\Omega$, motivated by (15) and the ideas of Becker and Rannacher [2, 4] we propose the following dual weighted-residual error estimator with $\|\xi - \xi_h\|_{L_2(\Omega)}$ as the quantity of interest:

$$\begin{aligned}\eta_{DWR}^2 := \Big| \sum_{T\in\mathcal{T}_h} \int_T (\nabla\times\mathbf{f} - \alpha\xi_h)(\tilde{\zeta} - \zeta_h)dx \\ - \sum_{E\in\mathcal{E}_h} \int_E ([\![\mathbf{f} - \nabla\times\xi_h]\!]\cdot t_E)(\tilde{\zeta} - \zeta_h)ds\Big|.\end{aligned} \tag{19}$$

Here $\zeta_h \in V_h$ is the $P_1$ finite element solution of (14), where the unknown function $\xi$ is replaced by some higher order interpolant $\tilde{\xi}$ of $\xi_h$, and $\tilde{\zeta}$ is also a higher order interpolant of $\zeta_h$. Details of the interpolation scheme we use can be found in Section 3.

*Remark* 4. The reliability and efficiency of the error estimator $\eta_{DWR}$ will be demonstrated numerically in Section 4. We note that the theoretical justification of dual weighted-residual error estimators has been discussed in [12, 24].

## 3. An Adaptive Finite Element Method

The adaptive finite element method (AFEM) creates a sequence of nested triangulations $\mathcal{T}_0, \mathcal{T}_1, \mathcal{T}_2, \ldots$ with associated $P_1$ finite element spaces

$$V_0 \subsetneq V_1 \subsetneq V_2 \subsetneq \ldots \subsetneq V_\ell \subset V = H^1(\Omega)$$

and discrete solutions $\mathbf{u}_\ell$ and $\xi_\ell$. It consists of the following loop

$$\text{Solve} \to \text{Estimate} \to \text{Mark} \to \text{Refine}.$$

3.1. **Solve.** We apply the following algorithm from [8] (cf. the description in Section 1 where $V_h = V_\ell$ and $\mathring{V}_h = \mathring{V}_\ell \cap H_0^1(\Omega)$) to compute the discrete solutions $\mathbf{u}_\ell$ and $\xi_\ell$ on the mesh $\mathcal{T}_\ell$.

(1) Compute a numerical approximation $\xi_\ell \in V_\ell$ of $\xi = \nabla\times\mathbf{u}$ by solving (6) when $\alpha \neq 0$, and by (6) together with the constraint $(\xi_\ell, 1) = 0$ when $\Omega$ is simply connected and $\alpha = 0$.
(2) Compute a numerical approximation $\phi_\ell \in V_\ell$ of $\phi$ by solving (7) under the constraint $(\phi_\ell, 1) = 0$.
(3) If $\Omega$ is not simply connected, compute numerical approximations $\varphi_{1,\ell}, \ldots, \varphi_{m,\ell} \in V_\ell$ of $\varphi_1, \ldots, \varphi_m$ by solving (8), and compute numerical approximations $c_{1,\ell}, \ldots, c_{m,\ell}$ of $c_1, \ldots, c_m$ by solving (9).
(4) The approximation of $\mathbf{u}$ is given by (cf. (10))

$$\mathbf{u}_\ell = \nabla\times\phi_\ell + \sum_{j=1}^{m} c_{j,\ell}\nabla\varphi_{j,\ell}.$$

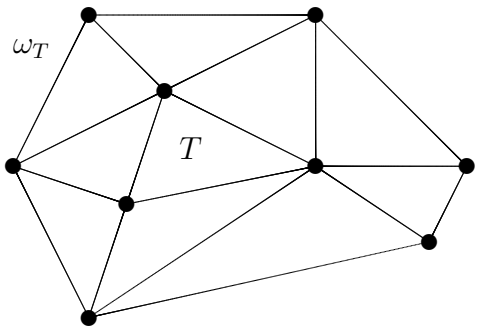


FIGURE 1. Example of an element patch. The sampling points are all vertices.

3.2. **Estimate.** Based on the discrete solutions $\mathbf{u}_\ell$ and $\xi_\ell$ the errors $\|\mathbf{u}-\mathbf{u}_\ell\|_{L_2(\Omega)}$ and $\|\xi-\xi_\ell\|_{L_2(\Omega)}$ are estimated with the *a posteriori* error estimators of Section 2.

The error $\|\mathbf{u}-\mathbf{u}_\ell\|_{L_2(\Omega)}$ is estimated by $\eta_R$ (cf. (13)) with the (local) refinement indicators

$$\eta_{\ell,R}^2(T) := h_T^2\|\xi_\ell\|_{L_2(T)}^2 + \frac{1}{2}\sum_{E\subset\partial T} h_E\|[\![\nabla\times\phi_\ell]\!]\cdot t_E\|_{L_2(E)}^2 + \frac{1}{2}\sum_{j=1}^{m}\sum_{E\subset\partial T\setminus\partial\Omega} h_E\|[\![\nabla\varphi_{j,\ell}]\!]\cdot n_E\|_{L_2(E)}^2,$$

where the higher order term $\|\xi-\xi_\ell\|_{L_2(\Omega)}$ is ignored.

The error $\|\xi-\xi_\ell\|_{L_2(\Omega)}$ is estimated by $\eta_{reg}$ (cf. (18)) with the (local) refinement indicators

$$\eta_{\ell,reg}^2(T) := h_T^4\|\nabla\times\mathbf{f}-\alpha\xi_\ell\|_{L_2(T)}^2 + \frac{1}{2}\sum_{E\subset\partial T} h_E^3\|[\![\mathbf{f}-\nabla\times\xi_\ell]\!]\cdot t_E\|_{L_2(E)}^2,$$

or by $\eta_{DWR}$ (cf. (19)) with the (local) refinement indicators

$$\eta_{\ell,DWR}^2(T) := \Big|\int_T(\nabla\times\mathbf{f}-\alpha\xi_\ell)(\tilde{\zeta}-\zeta_\ell)dx - \frac{1}{2}\sum_{E\subset\partial T}\int_E([\![\mathbf{f}-\nabla\times\xi_\ell]\!]\cdot t_E)(\tilde{\zeta}-\zeta_\ell)ds\Big|.$$

Here $\zeta_\ell\in V_\ell$ denotes the solution of the discrete dual problem

$$(\nabla\times\zeta_\ell,\nabla\times v_\ell)+\alpha(\zeta_\ell,v_\ell)=(\tilde{\xi}-\xi_\ell,v_\ell)\quad\forall v_\ell\in V_\ell$$

that satisfies the constraint $(\zeta_\ell,1)=0$, and the functions $\tilde{\xi}$ and $\tilde{\zeta}$ are higher order interpolants of $\xi_\ell$ and $\zeta_\ell$ constructed by the $L_2$ averaging technique of [28].

In the first step of the construction of $\tilde{\xi}$ a higher order interpolation $\hat{\xi}\in P_2(T)$ is computed from $\xi_\ell$ for each element $T\in\mathcal{T}_\ell$ separately. The values for the interpolated function at the vertices and midpoints

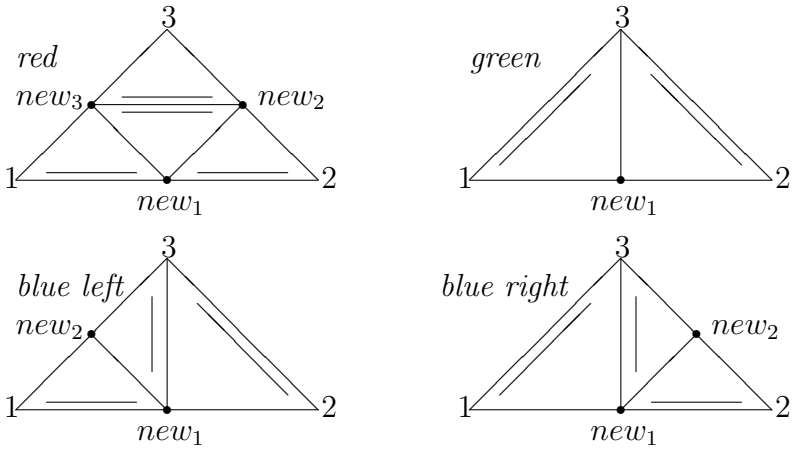


FIGURE 2. Refinement rules: sub-triangles with corresponding reference edges depicted with a second edge.

of the edges for an element $T \in \mathcal{T}_\ell$ are determined by a least squares approximation of a global quadratic polynomial on the element patch $\omega_T := \cup_{K\in\mathcal{T}_\ell, T\cap K\neq\emptyset} K$ as depicted in Figure 1. The sampling points for the least squares interpolation are chosen to be all the vertices of the element patch.

In the second step, a smooth interpolant $\tilde{\xi} \in P_2(\mathcal{T}_\ell)$ is obtained by taking the average of $\hat{\xi}$ over the nodal patch $\omega_z := \cup_{K\in\mathcal{T}_\ell, z\in K} K$ for the degree of freedom at the vertex $z$:

$$\tilde{\xi}(z) = \frac{1}{|T \in \mathcal{T}_\ell, T \subseteq \omega_z|} \sum_{T\in\mathcal{T}_\ell, T\subseteq\omega_z} \hat{\xi}(z)|_T,$$

and by taking the average of $\hat{\xi}$ over the edge patch $\omega_E := \cup_{K\in\mathcal{T}_\ell, E\subset K} K$ for the degree of freedom at the midpoint $m_E$ of E:

$$\tilde{\xi}(m_E) = \frac{1}{|T \in \mathcal{T}_\ell, T \subseteq \omega_E|} \sum_{T\in\mathcal{T}_\ell, T\subseteq\omega_E} \hat{\xi}(m_E)|_T.$$

The evaluation of $\tilde{\zeta}$ follows the same procedure. Numerical examples below indicate that the proposed procedure leads to reliable and efficient *a posteriori* error estimators.

3.3. **Mark.** Based on the refinement indicators, elements are marked for refinement in a bulk criterion [18] such that $\mathcal{M}_\ell \subseteq \mathcal{T}_\ell$ is a minimal set of marked elements with

$$\theta \sum_{T\in\mathcal{T}_\ell} \eta_\ell^2(T) \leq \sum_{T\in\mathcal{M}_\ell} \eta_\ell^2(T),$$

for a bulk parameter $0 < \theta \leq 1$, where $\eta_\ell$ is either $\eta_{\ell,R}$, $\eta_{\ell,reg}$ or $\eta_{\ell,DWR}$. This is carried out by a greedy algorithm which marks elements with larger contributions.

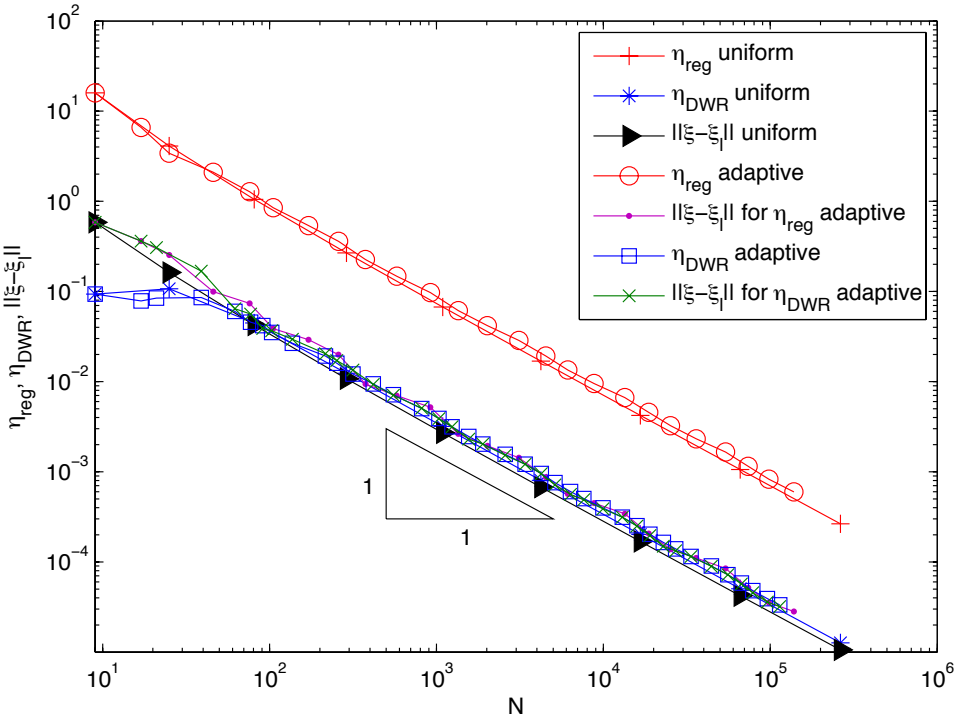


FIGURE 3. Convergence histories of $\|\xi - \xi_\ell\|_{L_2(\Omega)}$, $\eta_{reg}$ and $\eta_{DWR}$ on uniformly and adaptively refined meshes for the unit square example.

3.4. **Refine.** The mesh is refined locally using the set $\mathcal{M}_\ell$ of marked elements. Once an element is selected for refinement, all of its edges are marked for refinement. In order to preserve the quality of the mesh, additional edges are marked by the closure algorithm. For each triangle let one edge be the uniquely defined reference edge $E(T)$. The closure algorithm computes a superset of marked edges, such that once an edge of a triangle $T \in \mathcal{T}_\ell$ is marked for refinement, its reference edge $E(T)$ is marked as well. After the closure algorithm is applied, triangles with marked edges are refined by one of the refinement rules depicted in Figure 2.

## 4. Numerical Examples

In this section we present the results of several numerical experiments. The reliability and efficiency of the error estimators for uniformly and adaptively refined meshes are verified for several examples using different domains and different values for $\alpha$. We also compare the new numerical approach with the discretization by the lowest order edge element in Nédélec's first family [23].

4.1. **Unit Square Example.** As the first example we consider problem (1) for $\alpha = 1$ on the unit square $\Omega = (0,1)^2$ and with right-hand

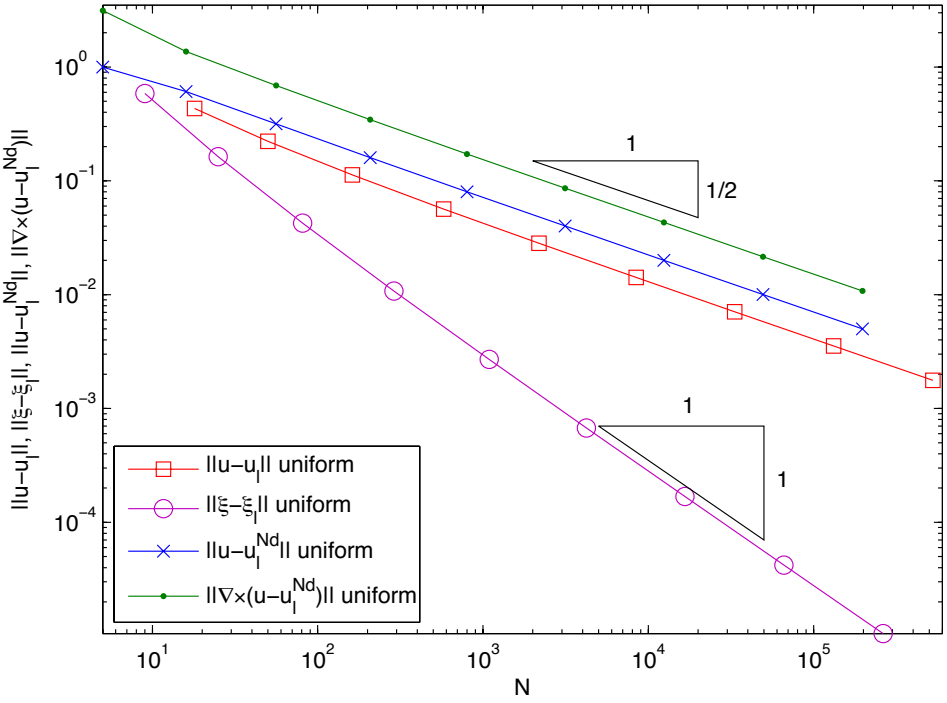


FIGURE 4. Comparison between the new numerical approach with errors $\|\mathbf{u} - \mathbf{u}_\ell\|_{L_2(\Omega)}$ and $\|\xi - \xi_\ell\|_{L_2(\Omega)}$ and the discretization by the lowest order edge element with errors $\|\mathbf{u} - \mathbf{u}_\ell^{Nd}\|_{L_2(\Omega)}$ and $\|\nabla \times (\mathbf{u} - \mathbf{u}_\ell^{Nd})\|_{L_2(\Omega)}$.

side $\mathbf{f}$ such that the smooth solution is given by

$$u(x, y) = (\sin \pi y, \sin \pi x).$$

Note that in this example $\Omega$ is simply connected and thus $\mathbf{u} = \nabla \times \phi$ and $\mathbf{u}_\ell = \nabla \times \phi_\ell$.

The convergence histories of $\|\xi - \xi_\ell\|_{L_2(\Omega)}$ using $\eta_{reg}$ or $\eta_{DWR}$ as the refinement indicator are displayed in Figure 3. Since the domain is convex, the estimate (17) for the *a posteriori* error estimator $\eta_{reg}$ is valid. The numerical results in Figure 3 indicate that both error estimators $\eta_{reg}$ and $\eta_{DWR}$ are empirical reliable and efficient for uniformly and adaptively refined meshes, and that the adaptive meshes with $\eta_{reg}$ or $\eta_{DWR}$ as refinement indicators lead to similar errors for $\|\xi - \xi_\ell\|_{L_2(\Omega)}$. Thus the proposed interpolation scheme for $\eta_{DWR}$ is numerically stable. The error estimator $\eta_{DWR}$ also seems to be almost exact.

Since the solution $\xi$ is smooth, the convergence rate for $\|\xi - \xi_\ell\|_{L_2(\Omega)}$ is numerically of optimal order $\mathcal{O}(N_\ell^{-1})$ as predicted by [8, Lemma 4.1] for both uniform and adaptive meshes, where $N_\ell$ is the dimension of $V_\ell$. Note that for uniform meshes $\mathcal{O}(N_\ell^{-1/2}) \approx h_\ell$.

The numerical results displayed in Figure 4 provide a comparison between the approximation $\mathbf{u}_\ell \in V_\ell$ based on the Hodge decomposition

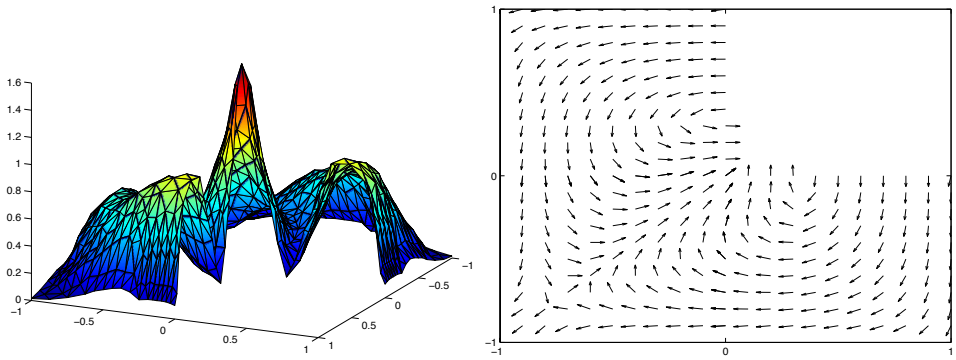

FIGURE 5. Plots of $|\mathbf{u}_\ell|_2$ (left) and the vector field $\mathbf{u}_\ell$ (right) for the L-shaped domain example.

and the approximation $\mathbf{u}_\ell^{Nd} \in V_\ell^{Nd}$ based on the lowest order edge element on uniform meshes, where $V_\ell^{Nd}$ is defined by

$$V_\ell^{Nd} := \Big\{ v \in H(\mathrm{curl};\Omega) : (v|_T)(x) = \begin{bmatrix} a_{T,1} \\ a_{T,2} \end{bmatrix} + b_T \begin{bmatrix} -x_2 \\ x_1 \end{bmatrix}, \\ a_{T,1}, a_{T,2}, b_T \in \mathbb{R}, \forall T \in \mathcal{T}_\ell \Big\}.$$

Even after taking into account that the computation of the vector field $\mathbf{u}_\ell$ requires the solution of two scalar elliptic problems (i.e., the error $\|\mathbf{u} - \mathbf{u}_\ell\|_{L_2(\Omega)}$ is plotted versus the degrees of freedom $2N_\ell$), the new approach shows a slightly smaller error in the vector field variable than the edge element. The error $\|\xi - \xi_\ell\|_{L_2(\Omega)}$ for the new approach is of one order higher than $\|\nabla \times (\mathbf{u} - \mathbf{u}_\ell^{Nd})\|_{L_2(\Omega)}$ for the edge element and therefore much smaller for larger degrees of freedom. Hence the proposed scheme leads empirically to comparable or better results than the lowest order edge element discretization.

4.2. **L-Shaped Domain Example.** The second numerical example concerns the model problem (1) with $\alpha = -1$ on the L-shaped domain $\Omega = (-1,1)^2 \backslash [0,1]^2$. A singular solution in polar coordinates $(r,\theta)$ is given by

$$\mathbf{u} = \nabla \times \left( r^{2/3} \cos\left(\frac{2}{3}\theta - \frac{\pi}{3}\right) \phi(x) \right),$$

with $\phi(x) = (1 - x_2^2)^2 (1 - x_1^2)^2$. The corresponding right-hand side $\mathbf{f} \in H(\mathrm{div}^0;\Omega)$ is computed by $\mathbf{f} = \nabla \times (\nabla \times \mathbf{u}) - \mathbf{u}$. The Euclidean norm of $\mathbf{u}_\ell$ on an adaptive mesh based on $\eta_R$ and the vector fiels $\mathbf{u}_\ell$ on an uniform mesh are portrayed in Figure 5. For visualization purposes the discontinuous values for $|\mathbf{u}_\ell|_2$ have been smoothed by the arithmetic mean value at the vertices.

The convergence histories of the errors and the error estimators are reported in Figure 6 and Figure 7. Since the domain is nonconvex, uniform refinement results in suboptimal convergence rates of $\mathcal{O}(N_\ell^{-1/3})$

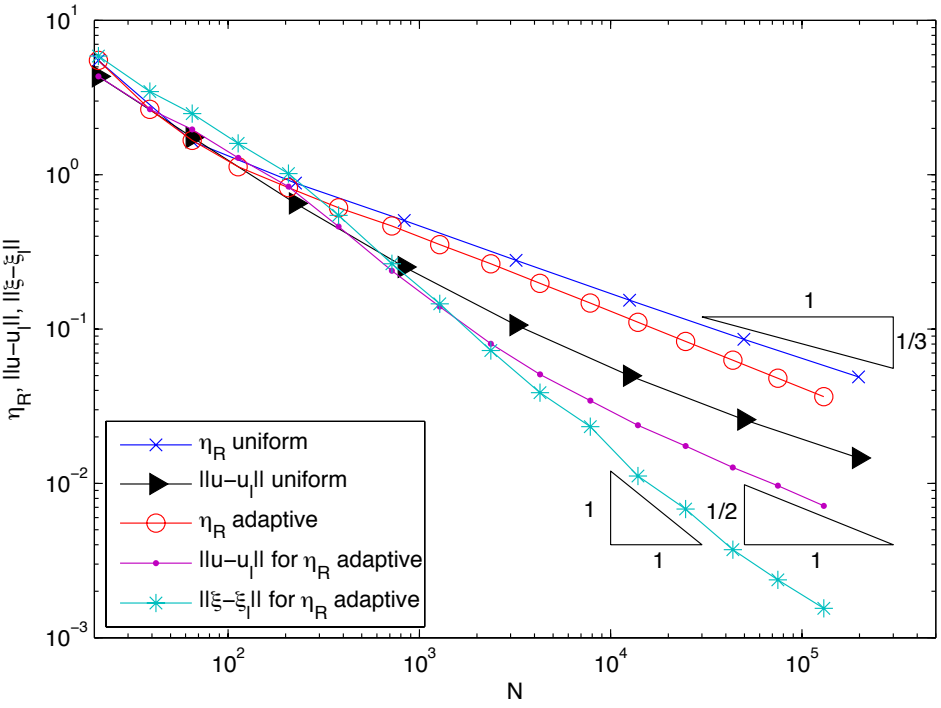


FIGURE 6. Convergence histories of $\|\mathbf{u}-\mathbf{u}_\ell\|_{L_2(\Omega)}$, $\|\xi-\xi_\ell\|_{L_2(\Omega)}$ and $\eta_R$ on uniformly and adaptively refined meshes for the L-shaped domain example.

for $\|\mathbf{u}-\mathbf{u}_\ell\|_{L_2(\Omega)}$ and $\mathcal{O}(N_\ell^{-2/3})$ for $\|\xi-\xi_\ell\|_{L_2(\Omega)}$ as predicted by [8, Theorem 4.9 and Lemma 4.1], while adaptive refinement leads to empirically optimal convergence rates of $\mathcal{O}(N_\ell^{-1/2})$ and $\mathcal{O}(N_\ell^{-1})$. Figure 6 indicates that the error estimator $\eta_R$ is empirically reliable and efficient for both uniform and adaptive meshes. It is observed that $\|\xi-\xi_\ell\|_{L_2(\Omega)}$ is of higher order for smaller $h_\ell \ll 1$ even for adaptively refined meshes based on $\eta_R$.

The numerical results displayed in Figure 7 indicate that $\eta_{reg}$ is less reliable than $\eta_{DWR}$ on the nonconvex L-shaped domain because of the significantly larger error $\|\xi-\xi_\ell\|_{L_2(\Omega)}$ for $\eta_{reg}$ on adaptive meshes. The error estimator $\eta_{DWR}$ is shown to be both reliable and efficient. Figure 8 depicts some adaptively refined meshes. All error estimators refine strongly towards the corner singularity at the origin. However, the mesh for $\eta_{reg}$ shows much less refinement at the origin which may produce larger errors in $\|\xi-\xi_\ell\|_{L_2(\Omega)}$.

The numerical results displayed in Figure 9 provide a comparison between the approximations based on the Hodge decomposition and adaptive meshes generated by the error estimators $\eta_R$ and $\eta_{DWR}$, and the approximations based on the lowest order edge element and adaptive meshes generated by the residual-based error estimator in [14].

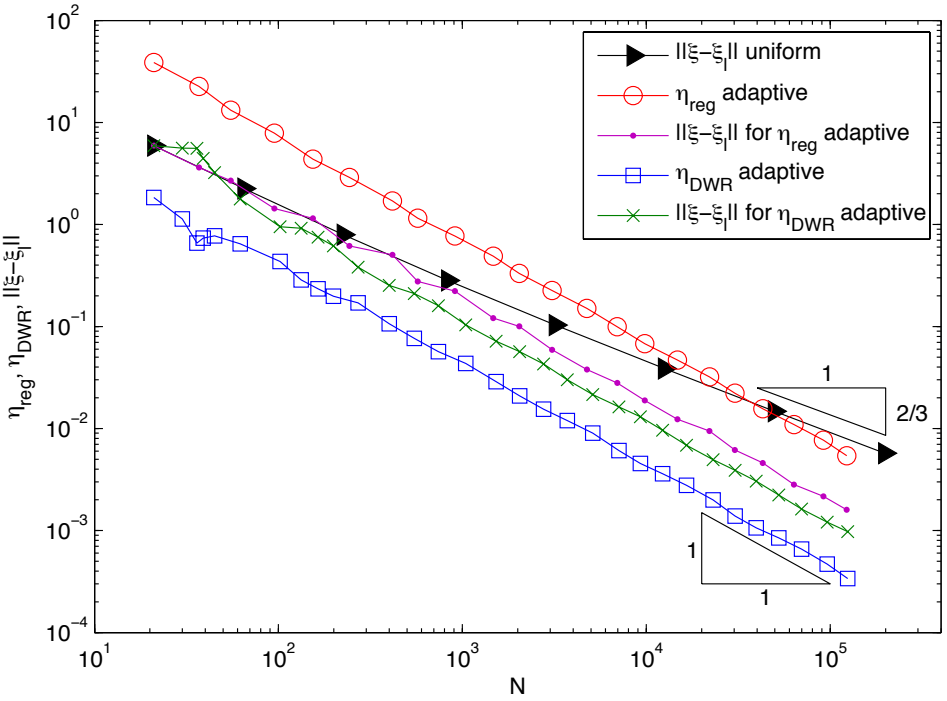


FIGURE 7. Convergence histories of $\|\xi - \xi_\ell\|_{L_2(\Omega)}$, $\eta_{reg}$ and $\eta_{DWR}$ on uniformly and adaptively refined meshes for the L-shaped domain example.

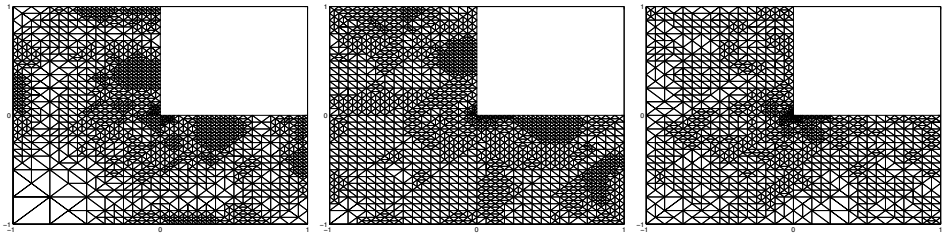

FIGURE 8. Adaptively refined meshes using the error estimators $\eta_R$, $\eta_{reg}$ and $\eta_{DWR}$ (from left to right) for the L-shaped domain example.

For a fair comparison we have plotted the errors $\|\mathbf{u} - \mathbf{u}_\ell\|_{L_2(\Omega)}$ versus $2N_\ell$. The numerical results show that adaptive mesh refinement leads to optimal convergence rates for both methods and that the new method leads asymptotically to smaller errors than the lowest order edge element method.

4.3. **Doubly Connected Domain Example.** The last example concerns the model problem (1) with $\alpha = 1$ on a doubly connected domain $\Omega = (0,4)^2 \backslash [1,3]^2$. Note that in this example $m = 1$ and therefore

$$\mathbf{u} = \nabla \times \phi + c\nabla\varphi.$$

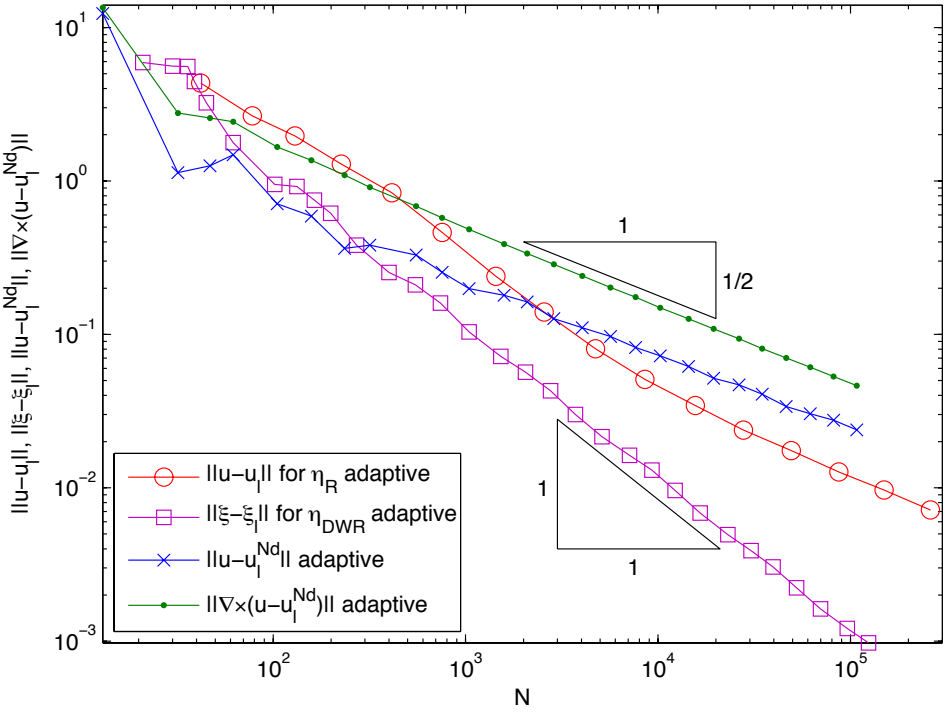


FIGURE 9. Comparison on adaptive meshes between the new numerical approach with errors $\|\mathbf{u}-\mathbf{u}_\ell\|_{L_2(\Omega)}$ and $\|\xi-\xi_\ell\|_{L_2(\Omega)}$ and the discretization by the lowest order edge element with errors $\|\mathbf{u}-\mathbf{u}_\ell^{Nd}\|_{L_2(\Omega)}$ and $\|\nabla\times(\mathbf{u}-\mathbf{u}_\ell^{Nd})\|_{L_2(\Omega)}$.

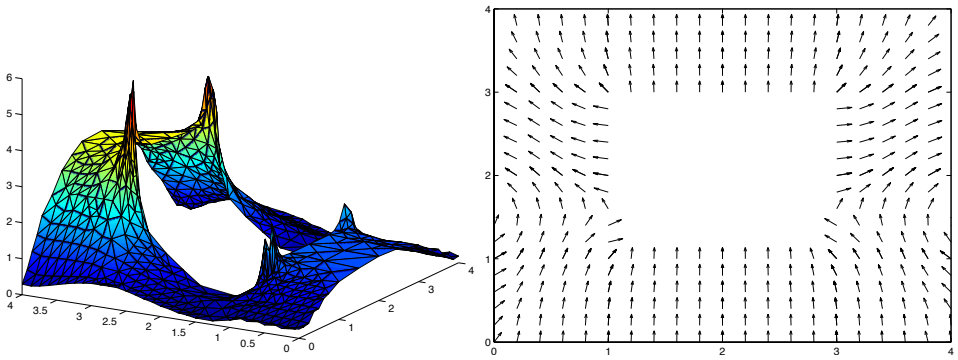

FIGURE 10. Plots of $|\mathbf{u}_\ell|_2$ (left) and the vector field $\mathbf{u}_\ell$ (right) for the doubly connected domain example.

The discontinuous right-hand side $\mathbf{f}$ is defined by

$$\mathbf{f} = \begin{cases} [1+x_1, 0] & \text{if } x_1 < x_2 \text{ and } 3 < x_1 < 4, \\ [0, 1+x_2] & \text{otherwise.} \end{cases}$$

The norm of $\mathbf{u}_\ell$ on an adaptive mesh based on $\eta_R$ and the vector field $\mathbf{u}_\ell$ on an uniform mesh are displayed in Figure 10, and the convergence

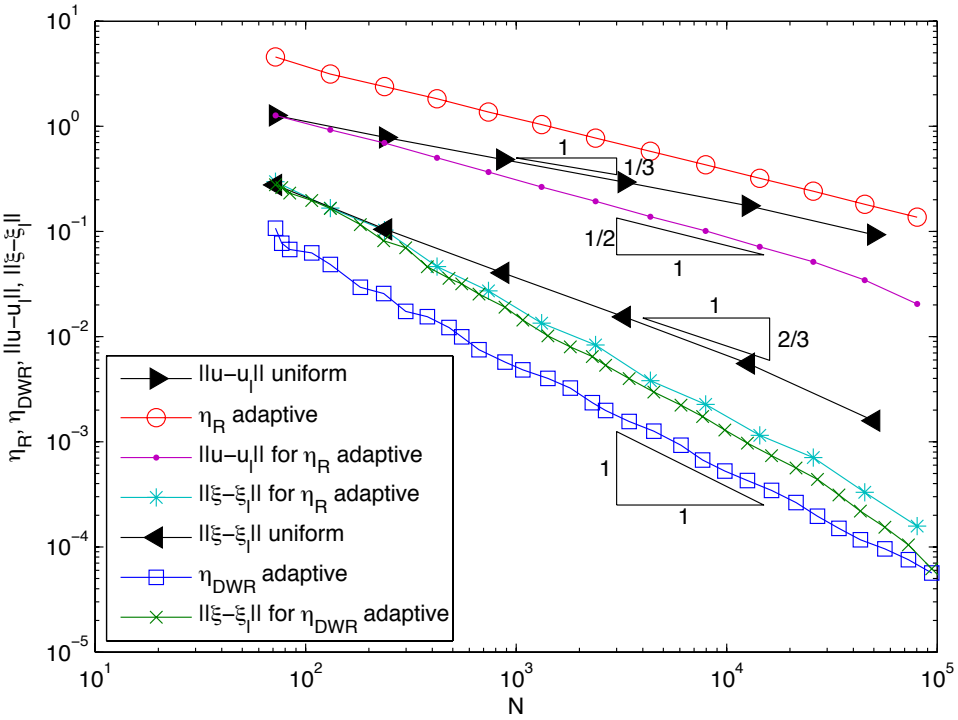


FIGURE 11. Convergence histories of $\|\mathbf{u} - \mathbf{u}_\ell\|_{L_2(\Omega)}$, $\|\xi - \xi_\ell\|_{L_2(\Omega)}$, $\eta_R$ and $\eta_{DWR}$ on uniformly and adaptively refined meshes for the doubly connected domain example.

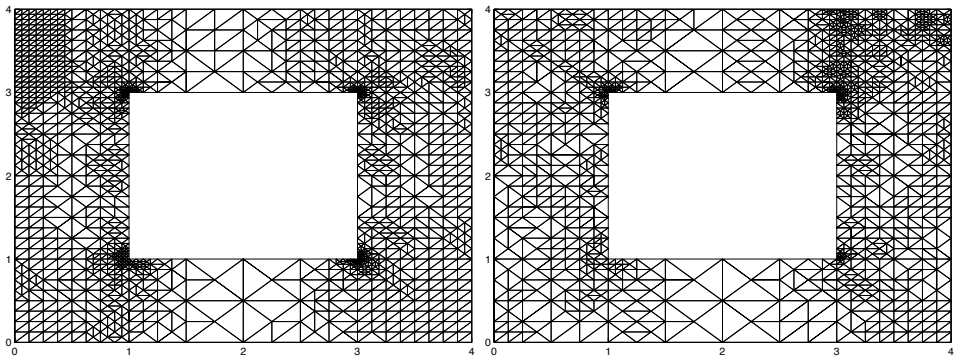

FIGURE 12. Adaptively refined meshes using the error estimators $\eta_R$ (left) and $\eta_{DWR}$ (right) for the doubly connected domain example.

histories of the errors and the error estimators are reported in Figure 11. Since the exact solution is not known, the errors are approximated by the difference between the discrete solution and the final grid solutions.

Note that the results displayed in Figure 11 indicate that this approximation of the error is sufficient except for the last few levels of

refinement. Since the domain is nonconvex, uniform refinement results in suboptimal convergence rates while adaptive refinement leads to empirically optimal convergence rates of $\mathcal{O}(N_\ell^{-1/2})$ and $\mathcal{O}(N_\ell^{-1})$ for the errors $\|\mathbf{u}-\mathbf{u}_\ell\|_{L_2(\Omega)}$ and $\|\xi-\xi_\ell\|_{L_2(\Omega)}$. The error estimators $\eta_R$ and $\eta_{DWR}$ are empirically reliable and efficient for adaptively refined meshes. The error $\|\xi-\xi_\ell\|_{L_2(\Omega)}$ is of higher order for $\eta_R$. Note that the error estimator $\eta_{DWR}$ underestimates the error $\|\xi-\xi_\ell\|_{L_2(\Omega)}$.

Figure 12 displays two adaptively refined meshes which are strongly refined at the four inner corners. The mesh for $\eta_{DWR}$ is additionally more refined in the area where the right-hand side $\mathbf{f}$ is discontinuous.

## 5. Concluding Remarks

We have developed an adaptive $P_1$ finite element method for two dimensional Maxwell's equations that is based on the Hodge/Helmholtz decomposition. In our experience the errors $\|\xi-\xi_\ell\|_{L_2(\Omega)}$ associated with the adaptive meshes based on the dual weighted-residual error estimator $\eta_{DWR}$ are slightly better than those associated with the residual error estimator $\eta_R$, while the errors $\|\mathbf{u}-\mathbf{u}_\ell\|_{L_2(\Omega)}$ behave in the opposite way. The overall performance of the two error estimators are comparable. Therefore between the two choices the adaptive method based on $\eta_R$ is recommended if one wants to approximate both $\mathbf{u}$ and $\xi=\nabla\times\mathbf{u}$, since the computational cost of $\eta_{DWR}$ is much higher.

For simplicity we set the electric permittivity and magnetic permeability to be 1. But the results in this paper can be extended to Maxwell's equations with general electric permittivity and magnetic permeability (cf. [8]).

## Acknowledgements

The bulk of this paper was written while the second author enjoyed the hospitality of the Center for Computation and Technology at Louisiana State University.

## References

1. M. Ainsworth and J. T. Oden, *A Posteriori Error Estimation in Finite Element Analysis*, Pure and Applied Mathematics, John Wiley and Sons, New York, 2000.
2. W. Bangerth and R. Rannacher, *Adaptive Finite Element Methods for Differential Equations*, Lectures in Mathematics ETH Zürich, Birkhäuser Verlag, Basel, 2003.
3. R. Beck, R. Hiptmair, R. H. W. Hoppe, and B. Wohlmuth, *Residual based a posteriori error estimators for eddy current computation*, M2AN. Mathematical Modelling and Numerical Analysis **34** (2000), no. 1, 159–182.
4. R. Becker and R. Rannacher, *A feed-back approach to error control in finite element methods: basic analysis and examples*, East-West Journal of Numerical Mathematics **4** (1996), no. 4, 237–264.

5. D. Braess and J. Schöberl, *Equilibrated residual error estimator for edge elements*, Math. Comp. **77** (2008), no. 262, 651–672.
6. S. C. Brenner and C. Carstensen, *Finite Element Methods*, Encyclopedia of Computational Mechanics (E. Stein, R. de Borst, and T. J. R. Hughes, eds.), John Wiley and Sons, Weinheim, Germany, 2004, pp. 73—118.
7. S. C. Brenner, F. Li, and L.-Y. Sung, *A locally divergence-free nonconforming finite element method for the time-harmonic Maxwell equations*, Mathematics of Computation **76** (2007), no. 258, 573–595.
8. S.C. Brenner, J. Cui, Z. Nan, and L.-Y. Sung, *Hodge decomposition for divergence-free vector fields and two-dimensional Maxwell's equations*, Mathematics of Computation **81** (2012), no. 278, 643–659.
9. S.C. Brenner, F. Li, and L.-Y. Sung, *A locally divergence-free interior penalty method for two-dimensional curl-curl problems*, SIAM Journal on Numerical Analysis **46** (2008), no. 3, 1190–1211.
10. ———, *A nonconforming penalty method for a two-dimensional curl-curl problem*, Mathematical Models and Methods in Applied Sciences **19** (2009), no. 4, 651–668.
11. S.C. Brenner and L.R. Scott, *The Mathematical Theory of Finite Element Methods*, third ed., Texts in Applied Mathematics, vol. 15, Springer, New York, 2008.
12. C. Carstensen, *Estimation of higher Sobolev norm from lower order approximation*, SIAM J. Numer. Anal. **42** (2005), no. 5, 2136–2147.
13. ———, *A unifying theory of a posteriori finite element error control*, Numerische Mathematik **100** (2005), no. 4, 617–637.
14. C. Carstensen and R. H. W. Hoppe, *Convergence analysis of an adaptive edge finite element method for the 2D eddy current equations*, Journal of Numerical Mathematics **13** (2005), no. 1, 19–32.
15. ———, *Unified framework for an a posteriori error analysis of non-standard finite element approximations of H(curl)-elliptic problems*, Journal of Numerical Mathematics **17** (2009), no. 1, 27–44.
16. P. Ciarlet, *Augmented formulations for solving Maxwell equations*, Computer Methods in Applied Mechanics and Engineering **194** (2005), no. 2-5, 559–586.
17. P. G. Ciarlet, *The finite element method for elliptic problems*, Studies in Mathematics and its Applications, vol. 4, North-Holland Publishing Co., Amsterdam, 1978.
18. W. Dörfler, *A convergent adaptive algorithm for Poisson's equation*, SIAM Journal on Numerical Analysis **33** (1996), no. 3, 1106–1124.
19. P. Grisvard, *Elliptic problems in nonsmooth domains*, Monographs and Studies in Mathematics, vol. 24, Pitman, Boston, MA, 1985.
20. R. Hiptmair, *Finite elements in computational electromagnetism*, Acta Numerica **11** (2002), 237–339.
21. R. H. W. Hoppe and J. Schöberl, *Convergence of adaptive edge element methods for the 3D eddy currents equations*, Journal of Computational Mathematics **27** (2009), no. 5, 657–676.
22. P. Monk, *Finite Element Methods for Maxwell's Equations*, Oxford University Press, New York, 2003.
23. J.-C. Nédélec, *Mixed finite elements in* $\mathbb{R}^3$, Numerische Mathematik **35** (1980), no. 3, 315–341.
24. R. H. Nochetto, A. Veeser, and M. Verani, *A safeguarded dual weighted residual method*, IMA J. Numer. Anal. **29** (2009), no. 1, 126–140.
25. J. Schöberl, *A posteriori error estimates for Maxwell equations*, Mathematics of Computation **77** (2008), no. 262, 633–649.

26. L. R. Scott and S. Zhang, *Finite element interpolation of nonsmooth functions satisfying boundary conditions*, Mathematics of Computation **54** (1990), no. 190, 483–493.
27. R. Verfürth, *A Review of A Posteriori Error Estimation and Adaptive Mesh-Refinement Techniques*, Wiley and Teubner, Chichester, UK, 1996.
28. N.-E. Wiberg and X. D. Li, *Superconvergent patch recovery of finite-element solution and a posteriori $L_2$ norm error estimate*, Communications in Numerical Methods in Engineering **10** (1994), no. 4, 313–320.

(S.C. Brenner) Department of Mathematics and Center for Computation and Technology, Louisiana State University, Baton Rouge, LA 70803, USA
*E-mail address*: brenner@math.lsu.edu

(J. Gedicke) Institut für Mathematik, Humboldt-Universität zu Berlin, Unter den Linden 6, 10099 Berlin, Germany
*E-mail address*: gedicke@mathematik.hu-berlin.de

(L.-Y. Sung) Department of Mathematics and Center for Computation and Technology, Louisiana State University, Baton Rouge, LA 70803, USA
*E-mail address*: sung@math.lsu.edu